International Journal of Engineering Science 225 (2026) 104550

Contents lists available at ScienceDirect

International Journal of Engineering Science

journal homepage: www.elsevier.com/locate/ijengsci

Full length article

Solitary wave dynamics of chains of bistable tensegrity prisms

Rana Nazifi Charandabi [a,*], Andrea Micheletti [b], Fernando Fraternali [c]

[a] Department of Information Engineering, Electrical Engineering and Applied Mathematics, University of Salerno, 84084 Fisciano(SA), Italy
[b] Department of Civil Engineering and Computer Science Engineering, University of Rome Tor Vergata, 00133 Rome, Italy
[c] Department of Civil Engineering, University of Salerno, 84084 Fisciano(SA), Italy

ARTICLE INFO

Keywords:
Tensegrity structures
Bistable response
Solitary waves
Wave focusing

ABSTRACT

This work investigates the propagation of nonlinear mechanical waves in chains of bistable tensegrity prisms subjected to impact loading. The analyzed systems consist of all-bar tensegrity prism units exhibiting bistable axial force–displacement responses with either softening or stiffening behavior, alternated with lumped masses. Numerical simulations are performed on finite chains to examine the formation, propagation, and attenuation of strain waves. The chain composed of thick prisms displays a softening bistable response, leading to the propagation of compressive axial strain waves with oscillatory tails and progressive attenuation. In contrast, chains composed of slender prisms exhibit a stiffening bistable response and support the propagation of localized compression pulses accompanied by limited background oscillations. Unlike classical bistable mass–spring chains, the tensegrity systems considered here exhibit intrinsically coupled axial and twisting motions. Nevertheless, the numerical results show good qualitative agreement between the impact-induced dynamic response of the analyzed systems and existing results in the literature on solitary-wave dynamics in bistable one-dimensional lattices. The distinctive wave behavior of bistable tensegrity lattices highlights their potential for applications involving wave focusing and controlled energy transmission and localization.

1. Introduction

It is well established in the literature that tensegrity-based lattices, both in one dimension and in higher-dimensional configurations, can sustain the propagation of solitary disturbances generated by impulsive loading, owing to their pronounced geometric nonlinearity. Depending on the specific force–displacement response of each module, these systems may generate either highly localized compressive pulses (Amendola, 2023; de Castro Motta, Garanger et al., 2024) or rarefaction-type solitary waves (de Castro Motta, Placidi et al., 2024), the former typically associated with stiffening behavior and the latter with softening mechanisms. The peculiar propagation of these solitary waves has inspired advanced studies in nonlinear acoustics. Tensegrity systems with softening behavior convert compressive impacts into rarefaction waves with fading oscillatory tails (Herbold & Nesterenko, 2013), whereas stiffening architectures enable adaptive acoustic lenses that focus compression solitary waves in prescribed regions (Spadoni & Daraio, 2010).

This study aims to extend research on the solitary-wave dynamics of tensegrity lattices to chains of bistable tensegrity prisms, a direction preliminarily indicated in Vangelatos et al. (2020), which, however, did not provide a detailed mechanical analysis of the wave dynamics of such structures. The wave dynamics of bistable lattices has been widely investigated in the literature, and key results can be found in Katz and Givli (2018), Meaud and Che (2017), Nadkarni, Chong et al. (2016), Nadkarni, Daraio et al. (2016),

* Corresponding author.
E-mail addresses: rnazificharandabi@unisa.it (R. Nazifi Charandabi), micheletti@ing.uniroma2.it (A. Micheletti), f.fraternali@unisa.it (F. Fraternali).

https://doi.org/10.1016/j.ijengsci.2026.104550
Received 21 February 2026; Received in revised form 8 April 2026; Accepted 13 April 2026
Available online 22 April 2026

Nadkarni et al. (2014), Shiroky and Gendelman (2017), Truskinovsky and Vainchtein (2014) and Zhang and Rudykh (2024) and the references therein. However, the available one-dimensional studies cannot be directly applied to chains of tensegrity prisms owing to the coupled axial–twisting response exhibited by such systems under axial loading. There is therefore room for investigations specifically focused on the peculiar bistable wave dynamics of lattices with tensegrity architecture. The present work begins in Section 2 with an illustration of the bistable response of a tensegrity prism composed exclusively of bar members. The assembly of such units into a one-dimensional chain of bistable elements is presented in Section 3, which also describes the equations of motion adopted to investigate the wave dynamics of the chain and their numerical integration. Numerical results illustrating the distinctive solitary-wave dynamics of bistable tensegrity chains and their main features are reported in Section 4. Finally, Section 5 summarizes the principal findings of the study and outlines promising directions for future research.

2. Bistable response of an all-bar tensegrity prism

The so-called T3 tensegrity prism is surely among the most widely studied tensegrity units in the literature (Skelton & De Oliveira, 2009). It consists of three bars (or struts) and nine strings (or cables). Referring to the simplest configuration of such a system, six of the strings form two identical equilateral triangles that serve as terminal bases (base strings); three additional strings connect pairs of nodes on the two bases (cross strings); and three bars connect distinct pairs of nodes belonging to those bases. The geometry and kinematics of the prism are fully described by three parameters, namely the edge length ℓ of the terminal bases, the height h of the prism, defined as the distance between the centroids of the terminal base, and the twisting angle φ between the two bases (Fraternali et al., 2015). The T3 prism exhibits a single free-standing tensegrity configuration corresponding to a twisting angle of $5/6\pi$ between the terminal bases, which constitutes an infinitesimal mechanism and can be stabilized through the application of a state of self-stress. The latter is typically induced by the pretensioning of a cross string. It has been shown that such a system can be transformed into a bistable structure by replacing all the strings with bars connecting the same end nodes and by modifying the twisting angle of the freestanding configuration to $5/6\pi + \theta_0$, where θ_0 denotes a suitable value of the 'additional twisting angle' θ applied to the free-standing configuration (see Intrigila et al., 2022 and references therein). The resulting all-bar prism, hereafter again termed a T3 prism for brevity, even though it actually consists of 12 bars, admits a stable freestanding configuration under zero external load, hereafter referred to as SC_1. Once uniformly compressed, it attains a second stable configuration, SC_2, through a deformation process that passes through an unstable load-free configuration, UC. It can be shown that the second stable configuration SC_2 correspond to an additional twist $\theta = -\theta_0$.

Let us consider physical examples of bistable tensegrity prisms. Using the notation illustrated in Fig. 1(a), the position vectors of nodes 1–6 of these prisms in the SC_1 configuration can be expressed as follows

$$\boldsymbol{n}_i = \{a\cos[\psi(i-1)],\ a\sin[\psi(i-1)],\ 0\}, \qquad i = 1,2,3, \tag{1}$$

$$\boldsymbol{n}_{3+i} = \{a\cos[\psi(i-1)+\varphi],\ a\sin[\psi(i-1)+\varphi],\ h\}, \qquad i = 1,2,3 \tag{2}$$

where $\psi = 2/3\pi$; $a = \sqrt{3}\ell/3$ cm is the radius of the circumscribed circle to the triangular bases; and $\varphi = 5/6\pi + \theta_0$ is the relative twisting angle between the two bases.

The first physical model examined exhibits a 'thick' profile, characterized by the following design variables: $\ell = 13.260$ cm, $h = 7.588$ cm, and $\theta_0 = -10°$. This geometry is similar to that of the standard (non-bistable) thick prisms previously investigated in Fraternali et al. (2015).

The strongly nonlinear axial force F_d versus axial displacement d response of the thick bistable prism is shown in Fig. 2. Here, F_d denotes the total force applied to the terminal bases (i.e., the sum of the forces $F_d/3$ applied to the individual nodes), and d represents the relative axial displacement between these bases, measured from the reference configuration SC_1. Both quantities are taken as positive when the prism is in compression. The prism is equipped with circular bars of diameter 8 mm made of a thermoplastic polyurethane (TPU) characterized by a Young's modulus $E = 54$ MPa. The overall mass M of the prism, including the masses of the nodes, is estimated to be 0.25 kg. This mass is lumped at the terminal bases, which are assumed to be circular rings with radius $r = a$.

The axial F_d–d response shown in Fig. 2 was computed using the path-following procedure described in Fraternali et al. (2015), assuming a displacement-controlled loading scheme applied to a 3D model of the prism. In this loading condition, equal axial displacements are applied to the nodes of the top base in quasi-static increments of 0.125 mm, while the nodes of the bottom base are kept fixed. It is observed that the F_d–d response exhibits a positive slope at the stress-free configurations SC_1 and SC_2, attained at $d = 0$ and $d = 14.75$ mm, respectively, and a negative slope at the unstable configuration UC ($d = 6.125$ mm). The F_d–d curve also displays a positive peak at $d = 2.125$ mm, where $F_d = 4.556$ N, and a negative peak at $d = 10.375$ mm, where $F_d = -2.858$ N (Fig. 2).

Additional physical models examined in the present work exhibit a 'slender' profile. All such models are characterized by $\ell = 8.010$ cm, $\theta_0 = -10°$, and an overall mass M of 0.225 kg. We distinguish a 'slender 1' sample with $h = 32.520$ cm; a 'slender 2' sample with $h = 40.668$ cm; and a 'slender 3' sample with $h = 48.814$ cm. These prisms are fabricated from the same materials as the thick model. Their force–displacement responses, computed using the same procedure adopted for the thick prism under quasi-static increments of 0.015 mm in the relative axial displacement between the terminal bases, are illustrated in Fig. 3. These response laws exhibit a second stable configuration SC_2 for axial displacements ranging from 1.155 mm (slender 1 prism) to 0.765 mm, and an unstable configuration UC, reached for displacements varying from 0.555 mm (slender 1 prism) to 0.375 mm (slender 3 prism). The coordinates of the maximum points vary from (0.24 mm, 0.484 N) for the slender 1 prism to (0.165 mm, 0.222 N) for the slender 3

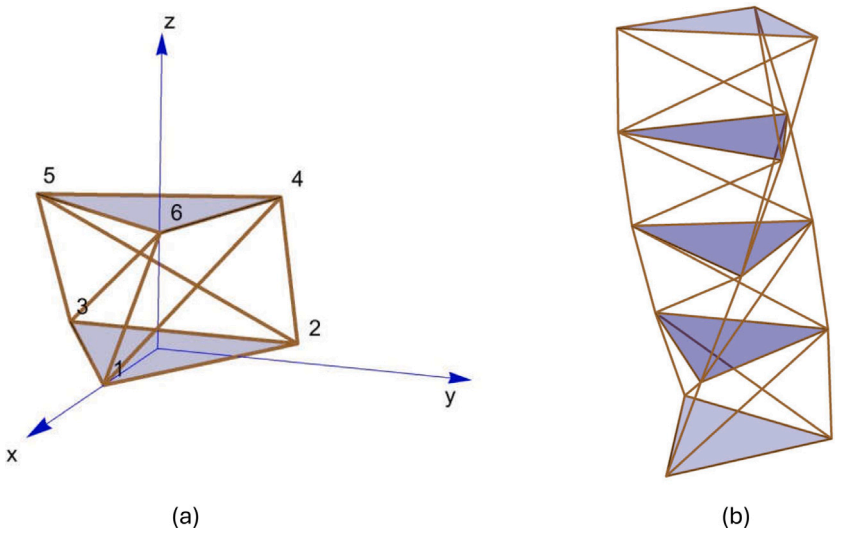

Fig. 1. Illustration of a T3 bistable prism (a) and a chain of bistable prisms (b).

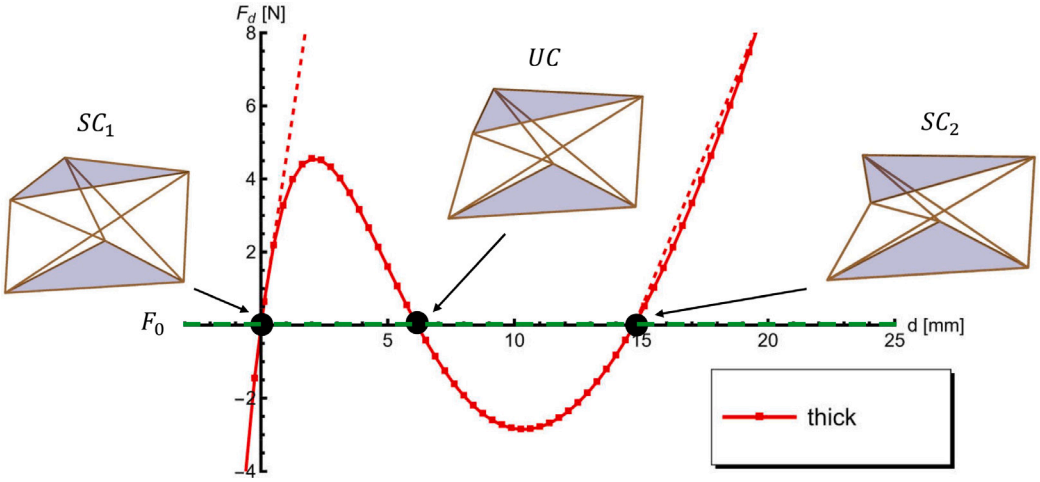

Fig. 2. Force–displacement plot of the examined thick bistable T3 prism. The linearizations adopted for stable Phases I and II are shown as dashed lines.

prism. The coordinates of the minimum points vary from (0.885 mm, −0.461 N) for the slender 1 prism to (0.6 mm, −0.210 N) for the slender 3 prism. It is observed that increasing the slenderness ratio h/ℓ leads to a smaller width of the spinodal region, defined as the interval between the maximum and minimum points of the force–displacement response (Katz & Givli, 2018).

It is important to note that the bistable tensegrity systems analyzed in this work exhibit coupled axial–twisting motions, whereas the bistable one-dimensional Fermi–Pasta– Ulam (FPU) lattices investigated in Katz and Givli (2018) exhibit purely axial motion. The presence of such coupling in tensegrity chains implies that they do not belong to the class of standard FPU lattices (Davini et al., 2016) (see also the observations in the next section). However, to enable qualitative comparisons between the present results and those reported in Katz and Givli (2018) for one-dimensional periodic mass–spring systems with a trilinear axial force–strain response, we linearize the two stable phases of the response laws shown in Figs. 2–3. Specifically, dashed lines represent the linearizations of the stable phases originating at the SC_1 and SC_2 configurations, hereafter referred to as Phase I and Phase II. The examined prisms exhibit an axial Maxwell force F_0 approximately equal to zero, i.e., the force at which the local energy minima associated with Phase I and Phase II are equal. Katz and Givli propose estimating the stiffness coefficients of an equivalent trilinear model by averaging the slope of the force–displacement response over the first stable branch below F_0 (Phase I) and the second stable branch above F_0 (Phase II). Since the present study focuses on compression waves, the equivalent axial stiffness of Phase I ($k_h^{(1)}$) is estimated as the tangent stiffness of the force–displacement curve at the SC_1 configuration. The stiffness of Phase II ($k_h^{(2)}$) is instead estimated as the secant stiffness along the initial portion of the second stable branch above the SC_2 configuration (see Figs. 2–3). Table 1 reports the resulting stiffness values, along with the stiffness ratio $\beta_2 = k_h^{(2)}/k_h^{(1)}$. The table also includes the corresponding

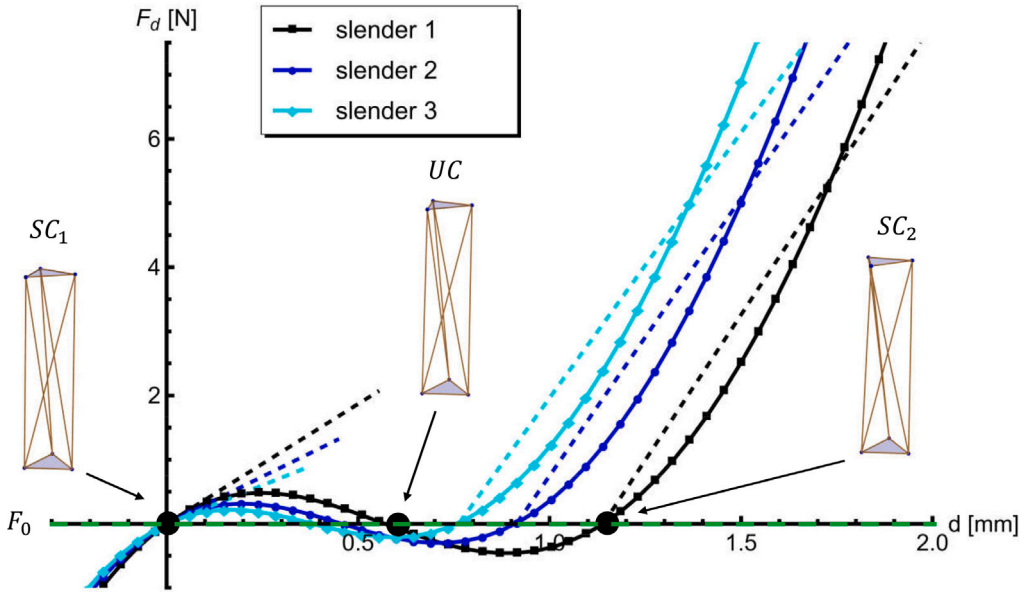

Fig. 3. Force–displacement plots of the examined slender 1, slender 2, and slender 3 bistable T3 prisms. The insets illustrate the key configurations of the slender 1 prism. The linearizations adopted for stable Phases I and II are shown as dashed lines.

Table 1
Effective constitutive parameters predicted for the examined prism chains.

Prism unit type	$k_h^{(1)}$ [N m]	$k_h^{(2)}$ [N m]	β_2	ε_{UC} [%]	$\Delta\varepsilon$ [%]
thick	4578.121	1684.84	0.368	8.072	19.439
slender 1	3736.059	9054.636	2.423	0.175	0.350
slender 2	2939.092	8659.700	2.946	0.111	0.225
slender 3	2395.175	8284.750	3.456	0.077	0.157

axial strain ε_{UC} at the unstable configuration UC and the transition strain $\Delta\varepsilon$. Axial strain is defined as the ratio between the current displacement d and the initial height h of the unit. In particular, $\Delta\varepsilon$ is defined through the difference between the displacements at which the line $F_d = F_0$ intersects the Phase I and Phase II branches of the force–displacement response, normalized by the height h (Katz & Givli, 2018). It is worth noting that the axial strain corresponding to the SC_1 configuration is equal to zero in the present systems.

The results presented in Table 1 indicate that the chains formed by thick prisms (hereafter also referred to as the 'thick' chain) exhibit a *softening* behavior, characterized by $\beta_2 < 1$, whereas the chains formed by slender 1, 2, and 3 prisms all exhibit a *stiffening* behavior, characterized by $\beta_2 > 1$. The physical examples of bistable T3 prisms examined in this section are adopted as unit cells of the one-dimensional chains investigated in the remainder of the paper (Fig. 1(b)). A detailed illustration of the bistable nature of the response of T3 prisms, together with their analogy to three-hinge systems, is provided in Intrigila et al. (2022).

3. Mechanical modeling of the wave dynamics of chains of bistable prisms

The two types of bistable unit, thick and slender, are assembled into one-dimensional chains in which adjacent units share one base and have the same chirality. In this study, the modeling assumptions and the equation of motion described in Micheletti (2025) are adopted. The structure can be modeled as a three-dimensional elastic network of axial springs connecting nodal masses. The position vectors $\boldsymbol{p}_i$, $i = 1, \ldots, n_n$, of all nodes in the chain structure are collected in the global vector $\boldsymbol{p} \in \mathbb{R}^{3n_n}$. Each node is assigned the same mass: $m = 0.083$ kg for the thick prism and $m = 0.075$ kg for the slender prisms. The bar connecting nodes i and j is assumed to be massless (lumped-mass model) and carries an axial force $t_{ij} = k_{ij}\left(l_{ij}(\boldsymbol{p}) - \bar{l}_{ij}\right)$, where $l_{ij}(\boldsymbol{p}) = |\boldsymbol{p}_i - \boldsymbol{p}_j|$ and $\bar{l}_{ij}$ denote the current length and the rest length of the bar, respectively, and $k_{ij} = EA/\bar{l}_{ij}$ is its axial stiffness. The vector equation of motion for the ith node, in the absence of external loads and neglecting damping (as well as any other dissipative effects), is obtained from the balance of inertial and elastic forces and can be written as

$$m\,\ddot{\boldsymbol{p}}_i + \sum_j t_{ij}\,\boldsymbol{e}_{ij} = \boldsymbol{0}\,, \tag{3}$$

Here, the summation extends over all nodes j connected to node i by a bar, $\boldsymbol{e}_{ij} = (\boldsymbol{p}_i - \boldsymbol{p}_j)/l_{ij}$ are the unit vectors defining the bar directions, and $\ddot{\boldsymbol{p}}_i$ denotes the acceleration of the ith node. The equations of motion of the entire structure can be expressed in

compact form as

$$M\ddot{p} + A(p)t(p) = 0, \tag{4}$$

where t collects the axial forces in the n_e bars, $A(p)$ is the $3n_n \times n_e$ equilibrium matrix at configuration p, mapping bar forces to nodal forces as $f = A(p)t$, and M is the diagonal mass matrix with nonzero entries equal to m.

The impulsive wave dynamics of the chains are obtained by supplementing the equations of motion (4) with suitable initial conditions on nodal positions and velocities, as specified in the next section. The initial configuration coincides with the undeformed, stress-free state of the chain at rest, while all nodal velocities are set to zero except for the three nodes belonging to one terminal base. In the absence of dissipative mechanisms, the total energy of the system is conserved throughout the motion. For interpretative purposes, it is convenient to emphasize that the bistable prisms considered in this study form three-dimensional lattice structures, in which each triangular base possesses nine independent degrees of freedom associated with the three translational motions of its nodal masses. The resulting motion is characterized by a coupling between relative axial displacements and twisting rotations of the terminal bases, induced by the chirality of the prisms (see, e.g., Fraternali et al. (2015) and Oppenheim and Williams (2000) and references therein). The axial strain and twisting angle profiles discussed in the next section are not primary kinematic variables, but are instead derived from the underlying three-dimensional lattice dynamics.

4. Numerical simulations

We performed numerical simulations of the wave dynamics of chains composed of 100 prisms of the typologies described in Section 2, namely the thick prism and the slender 1, slender 2, and slender 3 prism units. The chains are impacted at one end, corresponding to the right end in the plots shown hereafter, where the chains are depicted in a horizontal configuration for clarity. The nodes at the opposite (left) end of the chain are assumed to remain at rest (fixed extremity or 'wall'). The initial velocities of the nodes at the impacted end are prescribed so as to trigger the transition from the first stable configuration to the second stable configuration of the terminal prism. This transition occurs through a motion closely following the infinitesimal mechanism of the corresponding prism with $\theta_0 = 0$. To this end, the velocity vector at each node is imposed orthogonal to the axes of the bar and cross-string members connected to that node. For the chain composed of thick prisms, the inward (compressive) longitudinal component of the velocity at each node is set equal to $v_c = 0.45\,\mathrm{m/s}$, which results in a tangential component along the direction tangent to the circumscribed circle of the terminal base equal to $v_t = 1.34\,\mathrm{m/s}$. For the chains composed of slender prisms, the inward longitudinal component is set equal to $v_c = 0.10\,\mathrm{m/s}$, corresponding to values of v_t equal to $1.40\,\mathrm{m/s}$ (slender 1), $1.76\,\mathrm{m/s}$ (slender 2), and $2.10\,\mathrm{m/s}$ (slender 3).

The analytical study reported in Katz and Givli (2018) for one-dimensional FPU bistable lattices predicts the formation of solitary waves in stiffening systems and, conversely, a progressive attenuation of the impact-induced disturbance in softening systems after a wave forms at the impacted end. In stiffening systems, the propagating solitary waves exhibit a propagation speed bounded between the speeds of sound associated with the two stable phases, and a wave height that increases with increasing values of the transition strain $\Delta\varepsilon$. The results presented hereafter illustrate the dynamic response of the chains of bistable prisms analyzed in this study, in terms of axial strain waves and associated twist angle waves generated by impact loading. These quantities are obtained a posteriori from the solution of the wave dynamics problem for the three-dimensional lattice model described in the previous section. Specifically, the axial strain ε of a generic prism is computed as the average relative axial displacement of the nodes of its terminal bases, normalized by the initial height h, whereas the additional twist angle θ is evaluated from the relative rotation between the bases about the longitudinal axis, as determined from the nodal displacements. Both measures are defined with respect to the reference configuration, characterized by a twisting angle of $5/6\pi$ between the terminal bases. It is well established in the literature that, under simplifying assumptions (e.g., rigid bases and bars), the kinematics of tensegrity prisms can be reduced to a single effective degree of freedom (Fraternali et al., 2015; Oppenheim & Williams, 2000). However, such a reduction does not apply in the present case, as the prisms considered here exhibit different aspect ratios and their bars are made of deformable TPU. Consequently, the systems under investigation cannot be classified as standard one-dimensional FPU lattices.

Figs. 4 and 5 show the axial strain and the corresponding additional twist angle wave profiles obtained for the thick and slender 1 chains analyzed in the present work using the mechanical model described in Section 3. In these figures, the wave fields are examined before the main oscillations reach the fixed end of the chain. For the thick-prism chain, the impact generates a longitudinal mechanical wave characterized by a transition from motion about SC_1 to motion about SC_2, involving only the first units of the chain, as evidenced by the axial strain and additional twist angle wave profiles (Fig. 4). This phenomenon is accompanied by a disordered compressive perturbation about SC_1 that propagates along the chain and reduces to a low amplitude after traversing the initially impacted units. A markedly different response is observed for the chains composed of slender prism units shown in Fig. 5, whose axial force–displacement responses exhibit a stiffening bistable behavior. These systems support the formation and propagation of localized axial strain pulses in which the motion of the units involves transitions between SC_1 and SC_2, with limited attenuation, in qualitative agreement with the predictions reported in Katz and Givli (2018) for bistable FPU lattices. It can be observed that the peaks of the strain and additional twist wave profiles in Fig. 5 occur nearly at the same times. A spatiotemporal analysis of the strain waves exhibited by the chains composed of thick prisms and slender 1 prisms is presented in Fig. 6. The horizontal axis represents the time elapsed since impact, while the vertical axis denotes the unit (prism) number. Each horizontal curve illustrates the time evolution of the strain response in a single unit. In the stiffening system (Fig. 6(b)), composed of slender 1 prisms, the plot exhibits a well-defined diagonal band representing the propagation of a solitary wave with phase transition, which travels along the chain and reflects at the boundary. In contrast, in the softening system composed of thick prisms (Fig. 6(a)), weak

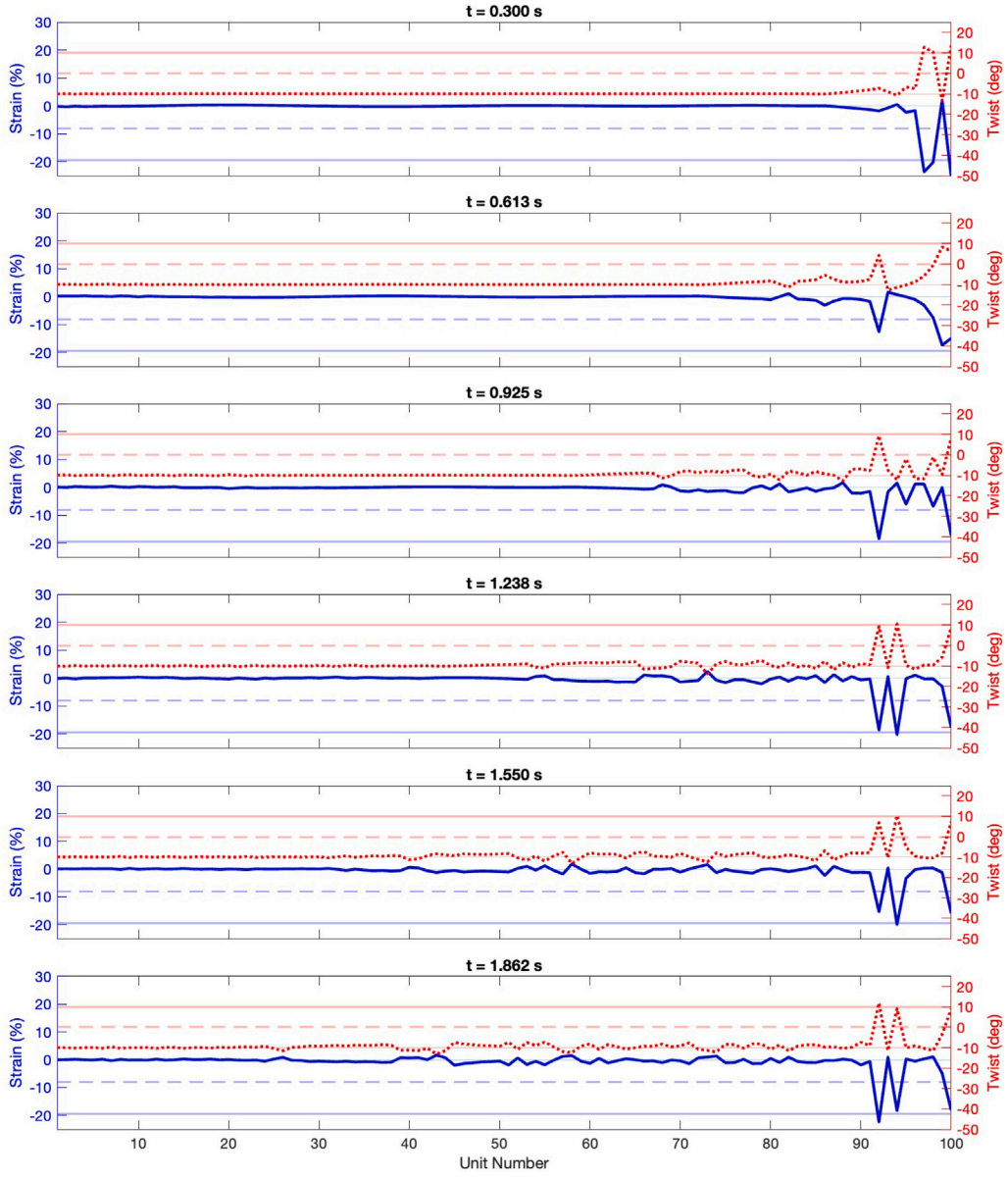

Fig. 4. Wave profiles of the axial strain (blue solid curves) and additional twist angle (red dotted curves) at different times in the chain composed of thick prisms, impacted at the right end with a uniform compressive velocity of 0.45 m/s. The horizontal dashed and solid lines indicate, respectively, the strain and twist angle values corresponding to the UC and SC_2 configurations.

waves propagate along the chain away from the impact point, while most of the deformation energy remains localized near the impact region (see also Fig. 4).

Figs. 7 and 8 further show the wave profiles obtained for the slender 2 and slender 3 chains, respectively. Among the examined stiffening bistable chains, we observe that the solitary wave propagating in the slender 1 chain exhibits the largest peak heights, consistent with the fact that this system is characterized by the largest transition strain $\Delta\varepsilon$. This wave is accompanied by minor strain oscillations both ahead of and behind the leading pulse (Fig. 5). The formation of a solitary pulse is further confirmed by the plots of the additional twist wave in Fig. 5, which show that the units carrying the pulse exhibit positive additional twist angles θ, whereas those not affected by the wave maintain $\theta = -10°$. The localized pulses propagating in the slender 2 and slender 3 chains exhibit more pronounced oscillations in the wave profiles, both ahead of and behind the leading pulse, compared to those observed in the slender 1 chain. Between these two cases, the slender 2 chain displays a larger peak amplitude and less pronounced oscillations than the slender 3 chain (see Figs. 7–8). In particular, the additional twist angle wave profiles of the chains composed

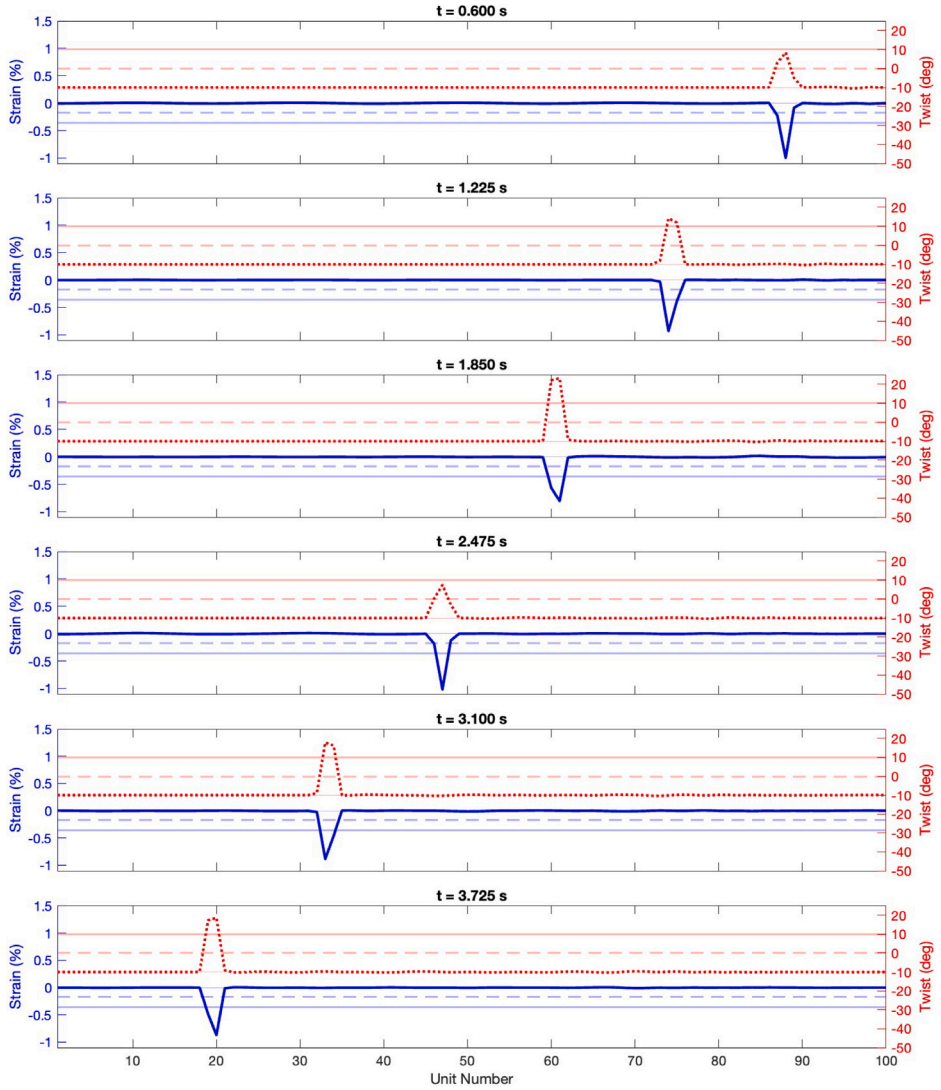

Fig. 5. Wave profiles of the axial strain (blue solid curves) and additional twist angle (red dotted curves) at different times in the chain composed of slender 1 prisms, impacted at the right end with a uniform compressive velocity of 0.1 m/s. The horizontal dashed and solid lines indicate, respectively, the strain and twist angle values corresponding to the UC and SC_2 configurations.

of slender 2 and slender 3 prisms exhibit a splitting of the main peak into two closely spaced peaks at certain time instants, as observed in Figs. 7–8.

In order to slightly strengthen the qualitative connection between the results obtained in this work and the predictions of Katz and Givli (2018), and with sole reference to deriving rough estimates of the sound speeds associated with the propagation of longitudinal waves in the linearized Phase I and Phase II, we adopt the approach proposed in Fraternali et al. (2025) for the linearized response of tensegrity chains characterized by coupled axial and twisting motions. This approach assumes that the relative angular velocity $\dot{\varphi}$ between the bases of a generic unit is related to the relative axial velocity $\dot{d}$ through a linear relation of the form

$$\dot{\varphi} = q\,\dot{d} \tag{5}$$

where q is a scalar coupling factor, which may take either positive or negative values. Making use of Eq. (5), the incremental dynamics of a generic unit cell, say the ith one, can be fully characterized in terms of the axial velocity $\dot{d}$, and the kinetic energy of the cell can be expressed in the form

$$K_i = \frac{1}{2} M \dot{d}_i^2 + \frac{1}{2} J \dot{\varphi}_i^2 = \frac{1}{2} M^{(eq)} \dot{d}_i^2 \tag{6}$$

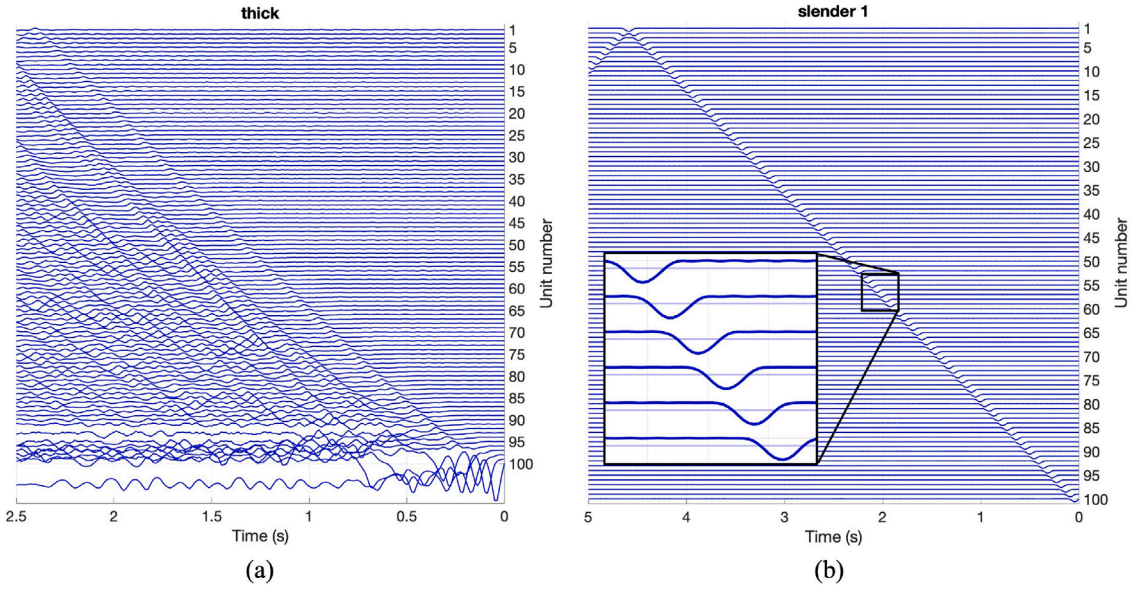

Fig. 6. Comparison of the spatiotemporal responses of chains composed of thick prisms (a) and slender 1 prisms (b) in terms of axial strain waves. The horizontal axis represents the time elapsed since the impact event, while the vertical axis denotes the prism number. The horizontally drawn curves illustrate the time evolution of the strain response in the individual units. The inset in panel (b) highlights a portion of the diagonal band associated with the propagation of a solitary wave with phase transition in the chain composed of slender 1 prisms.

In Eq. (6), $J = M r^2$ denotes the torsional moment of inertia of the unit, where r is the radius of the rings assumed to represent the lumped masses of the chain. The quantity M^{eq} is the equivalent mass, defined as

$$M^{(eq)} = M\left(1 + q^2 r^2\right) \tag{7}$$

We now particularize the above approach to the chain formed by slender 1 prisms. For this prism typology, we estimated a coupling factor q equal to $228.835\,\mathrm{m}^{-1}$ (in absolute value) in the linearized Phase I, which corresponds to an equivalent mass $M^{(eq,1)} = 25.423\,\mathrm{kg}$. In the linearized Phase II, the coupling factor is estimated as $q = 188.521\,\mathrm{m}^{-1}$, yielding an equivalent mass $M^{(eq,2)} = 17.327\,\mathrm{kg}$. According to this analysis, we estimated the speed of sound of longitudinal waves in Phase I as $c_1 = h\sqrt{k_h^{(1)}/M^{(eq,1)}} = 3.942\,\mathrm{m/s}$, and the speed of sound of longitudinal waves in Phase II as $c_2 = h\sqrt{k_h^{(2)}/M^{(eq,2)}} = 7.434\,\mathrm{m/s}$. Here, $h = 32.520\,\mathrm{cm}$ denotes the undeformed height of the prism under examination. By repeating the same analysis for the chain formed by slender 2 prisms, we obtained $c_1 = 2.826\,\mathrm{m/s}$ and $c_2 = 10.780\,\mathrm{m/s}$ ($h = 40.668\,\mathrm{cm}$, $M^{(eq,1)} = 60.850\,\mathrm{kg}$, and $M^{(eq,2)} = 12.324\,\mathrm{kg}$). Finally, for the chain formed by slender 3 prisms, we estimated $c_1 = 2.564\,\mathrm{m/s}$ and $c_2 = 15.393\,\mathrm{m/s}$ ($h = 48.814\,\mathrm{cm}$, $M^{(eq,1)} = 86.821\,\mathrm{kg}$, and $M^{(eq,2)} = 8.331\,\mathrm{kg}$). The propagation speed of the solitary pulse observed in Fig. 5 for the slender 1 chain is estimated to be $7.111\,\mathrm{m/s}$. The corresponding propagation speeds of the localized compression pulses observed in Figs. 7 and 8 for the slender 2 and slender 3 chains are estimated to be $8.459\,\mathrm{m/s}$ and $9.372\,\mathrm{m/s}$, respectively. In all cases, the measured propagation speeds fall within the corresponding intervals defined by c_1 and c_2, in qualitative agreement with the analysis presented in Katz and Givli (2018) for stiffening bistable lattices.

It is worth noting that the analytical expressions derived in this study for the wave peak amplitude cannot be directly applied to the chains examined here, as these systems do not constitute standard one-dimensional FPU lattices and exhibit different effective masses in Phase I and Phase II. An inspection of the results shown in Figs. 5–8 reveals that the axial strain solitary pulses propagating along the chains formed by slender 1, slender 2, and slender 3 prisms exhibit peak axial strains in the ranges $[0.9, 1.0]\%$, $[0.6, 0.8]\%$, and $[0.4, 0.5]\%$, respectively. Animations illustrating the motions exhibited by the examined chains are provided as Supplementary Materials.

5. Concluding remarks

This work has presented a numerical investigation of solitary-wave dynamics in one-dimensional chains of bistable tensegrity prisms. By exploiting the intrinsic bistability of all-bar T3 tensegrity units and their pronounced geometric nonlinearity, the study demonstrates the emergence of localized compression waves under impact loading, whose characteristics depend critically on whether the underlying force–displacement response is softening or stiffening. The examined chain formed by thick prisms exhibits a softening bistable behavior, leading to the generation of compression waves with oscillatory tails and progressively decreasing

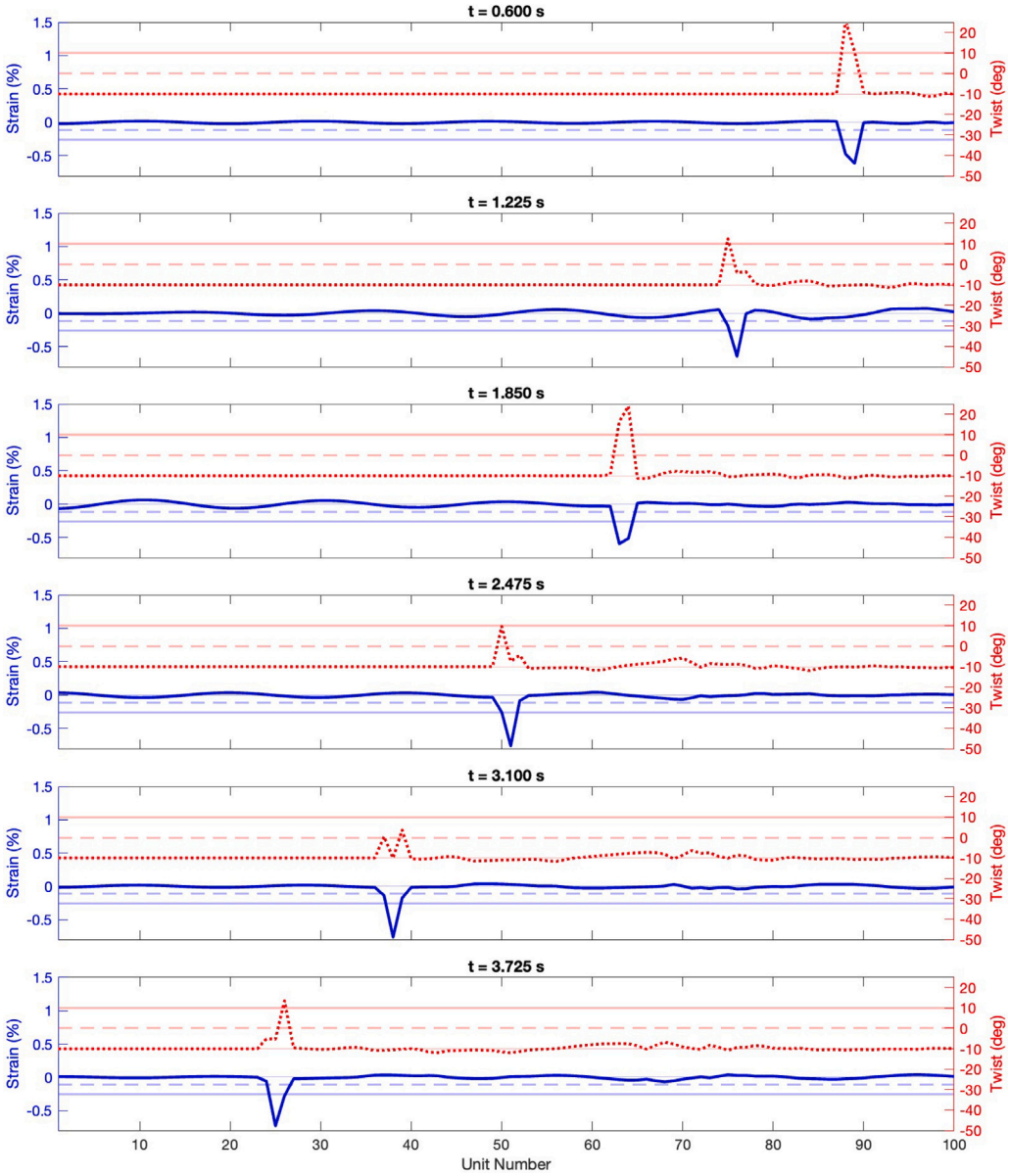

Fig. 7. Wave profiles of the axial strain (blue solid curves) and additional twist angle (red dotted curves) in the chain composed of slender 2 prisms, impacted at the right end with a uniform compressive velocity of 0.1 m/s.

amplitude. In contrast, chains composed of slender prisms display a stiffening bistable response and support the formation and propagation of compression solitary pulses with limited attenuation, accompanied by weak background oscillations. The main findings are in qualitative agreement with analytical predictions previously reported for one-dimensional bistable mass–spring lattices, despite the fundamental differences between the present tensegrity systems and classical axial lattices, which primarily arise from the spatial nature of tensegrity chains and the coupling between axial and twisting motions.

The present study opens several directions for future research, particularly toward the development of analytical models specifically tailored to the wave dynamics of bistable tensegrity systems, including the derivation of closed-form or asymptotic solutions for solitary-wave propagation in the presence of coupled axial and twisting motions. Further work should also explore the potential of bistable tensegrity chains as mechanical waveguides capable of transmitting and focusing energy through highly localized waveforms, as well as the experimental validation of the predicted wave phenomena under controlled impact and boundary conditions. These features make bistable tensegrity systems promising candidates for applications in mechanical-wave focusing and targeted energy delivery in engineered and biological materials.

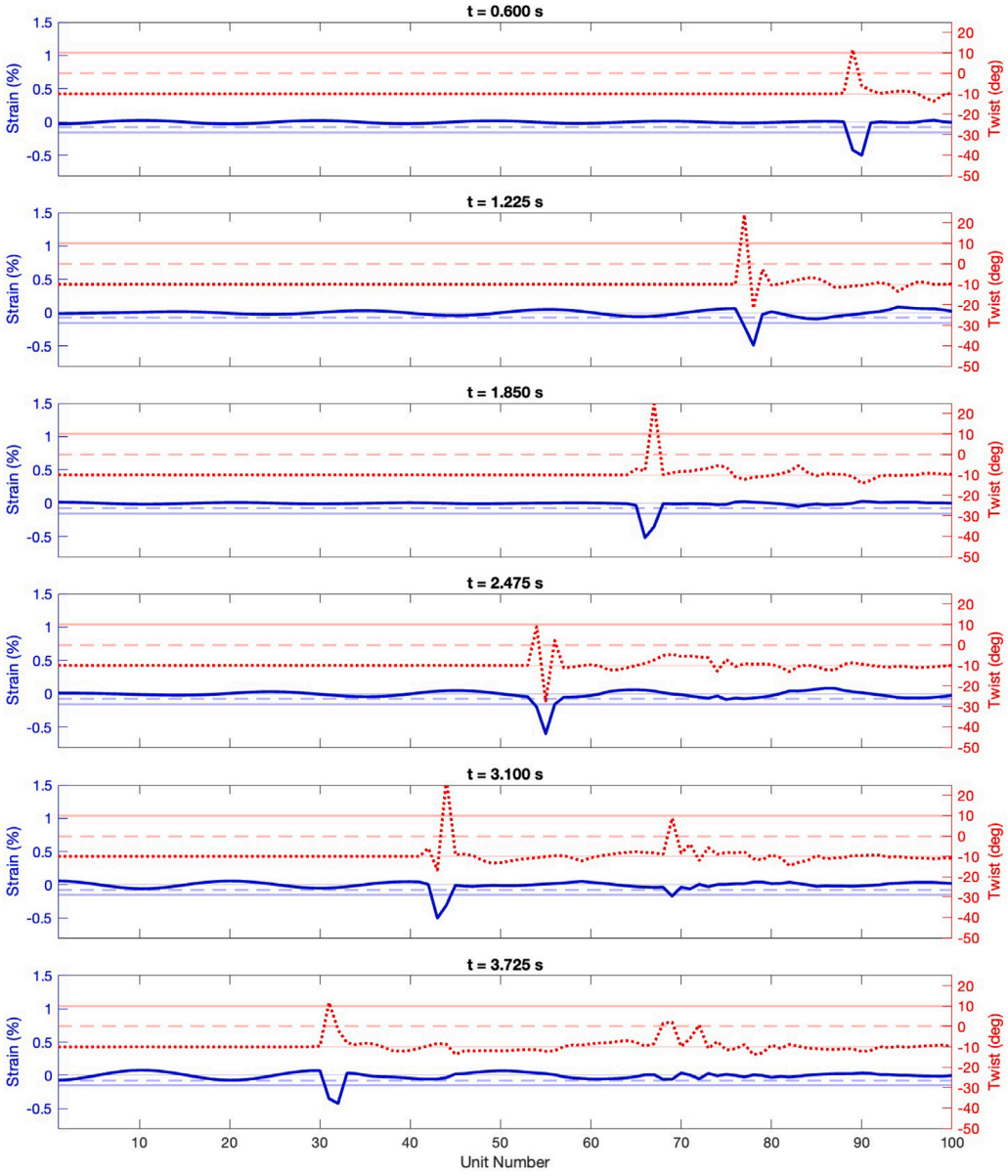

Fig. 8. Wave profiles of the axial strain (blue solid curves) and additional twist angle (red dotted curves) in the chain composed of slender 3 prisms, impacted at the right end with a uniform compressive velocity of 0.1 m/s.

CRediT authorship contribution statement

Rana Nazifi Charandabi: Writing – review & editing, Writing – original draft, Visualization, Validation, Supervision, Software, Resources, Project administration, Methodology, Investigation, Formal analysis, Data curation, Conceptualization. **Andrea Micheletti:** Writing – review & editing, Writing – original draft, Visualization, Validation, Supervision, Software, Resources, Project administration, Methodology, Investigation, Formal analysis, Data curation, Conceptualization. **Fernando Fraternali:** Writing – review & editing, Writing – original draft, Visualization, Validation, Supervision, Software, Resources, Project administration, Methodology, Investigation, Funding acquisition, Formal analysis, Data curation, Conceptualization.

Funding

FF and RNC acknowledge support by the Italian Ministry of Foreign Affairs and International Cooperation within the Italy-USA Science and Technology Cooperation Program 2023–2025, Project 'Next-generation green structures for natural disaster-proof buildings', grant number US23GR15.

Declaration of competing interest

The authors declare that they have no known competing financial interests or personal relationships that could have appeared to influence the work reported in this paper.

Appendix A. Supplementary data

Supplementary material related to this article can be found online at https://doi.org/10.1016/j.ijengsci.2026.104550.

Data availability

Data will be made available on request.

References

Amendola, A. (2023). An analytic study on the properties of solitary waves traveling on tensegrity-like lattices. *International Journal of Non-Linear Mechanics*, *148*, Article 104264.

Davini, C., Micheletti, A., & Podio-Guidugli, P. (2016). On the impulsive dynamics of T3 tensegrity chains. *Meccanica*, *51*, 2763–2776.

de Castro Motta, J., Garanger, K., & Rimoli, J. J. (2024). Propagation of compression solitary waves on tensegrity-like lattices made of truncated octahedrons. *International Journal of Non-Linear Mechanics*, *162*, Article 104716.

de Castro Motta, J., Placidi, L., Nazifi Charandabi, R., & Fraternali, F. (2024). A Weierstrass approach to the analysis of rarefaction solitary waves in tensegrity mass-spring systems. *Communications in Applied and Industrial Mathematics*, *15*(2), 8–16.

Fraternali, F., Carpentieri, G., & Amendola, A. (2015). On the mechanical modeling of the extreme softening/stiffening response of axially loaded tensegrity prisms. *Journal of the Mechanics and Physics of Solids*, *74*, 136–157.

Fraternali, F., de Castro Motta, J., & Placidi, L. (2025). Bandgap wave dynamics of tensegrity lattices. In *Tensegrity systems: Basic concepts, mechanical metamaterials, Biotensegrity* (pp. 57–82). Springer.

Herbold, E. B., & Nesterenko, V. F. (2013). Propagation of rarefaction pulses in discrete materials with strain-softening behavior. *Physical Review Letters*, *110*(14), Article 144101.

Intrigila, C., Micheletti, A., Nodargi, N. A., Artioli, E., & Bisegna, P. (2022). Fabrication and experimental characterisation of a bistable tensegrity-like unit for lattice metamaterials. *Additive Manufacturing*, *57*, Article 102946.

Katz, S., & Givli, S. (2018). Solitary waves in a bistable lattice. *Extreme Mechanics Letters*, *22*, 106–111.

Meaud, J., & Che, K. (2017). Tuning elastic wave propagation in multistable architected materials. *International Journal of Solids and Structures*, *122*, 69–80.

Micheletti, A. (2025). Basic tensegrity concepts and calculation methods. In F. Fraternali, & J. J. Rimoli (Eds.), *Tensegrity systems: basic concepts, mechanical metamaterials, Biotensegrity* (pp. 1–44). Springer Nature Switzerland, http://dx.doi.org/10.1007/978-3-031-82283-4_1.

Nadkarni, N., Arrieta, A. F., Chong, C., Kochmann, D. M., & Daraio, C. (2016). Unidirectional transition waves in bistable lattices. *Physical Review Letters*, *116*(24), Article 244501.

Nadkarni, N., Daraio, C., Abeyaratne, R., & Kochmann, D. M. (2016). Universal energy transport law for dissipative and diffusive phase transitions. *Physical Review B*, *93*(10), Article 104109.

Nadkarni, N., Daraio, C., & Kochmann, D. M. (2014). Dynamics of periodic mechanical structures containing bistable elastic elements: From elastic to solitary wave propagation. *Physical Review E*, *90*(2), Article 023204.

Oppenheim, I. J., & Williams, W. O. (2000). Geometric effects in an elastic tensegrity structure. *Journal of Elasticity and the Physical Science of Solids*, *59*(1), 51–65.

Shiroky, I., & Gendelman, O. (2017). Propagation of transition front in bi-stable nondegenerate chains: Model dependence and universality. *Journal of the Mechanics and Physics of Solids*, *104*, 144–156.

Skelton, R. E., & De Oliveira, M. C. (2009). *Tensegrity systems*. Berlin: Springer.

Spadoni, A., & Daraio, C. (2010). Generation and control of sound bullets with a nonlinear acoustic lens. *Proceedings of the National Academy of Sciences*, *107*(16), 7230–7234.

Truskinovsky, L., & Vainchtein, A. (2014). Solitary waves in a nonintegrable Fermi-Pasta-Ulam chain. *Physical Review E*, *90*(4), Article 042903.

Vangelatos, Z., Micheletti, A., Grigoropoulos, C. P., & Fraternali, F. (2020). Design and testing of bistable lattices with tensegrity architecture and nanoscale features fabricated by multiphoton lithography. *Nanomaterials*, *10*(4), 652.

Zhang, Q., & Rudykh, S. (2024). Propagation of solitary waves in origami-inspired metamaterials. *Journal of the Mechanics and Physics of Solids*, *187*, Article 105626.